Carbohydrate Polymers 87 (2012) 274–283

Contents lists available at ScienceDirect

Carbohydrate Polymers

journal homepage: www.elsevier.com/locate/carbpol

Biocompatible alginate/nano bioactive glass ceramic composite scaffolds for periodontal tissue regeneration

Sowmya Srinivasan, R. Jayasree, K.P. Chennazhi, S.V. Nair, R. Jayakumar*

Amrita Centre for Nanosciences and Molecular Medicine, Amrita Institute of Medical Sciences and Research Centre, Amrita Vishwa Vidyapeetham University, Kochi 682 041, India

ARTICLE INFO

Article history:
Received 7 June 2011
Received in revised form 19 July 2011
Accepted 25 July 2011
Available online 3 August 2011

Keywords:
Alginate
Bioglass
Periodontal regeneration
Nanocomposite
Alkaline phosphatase
Tissue engineering

ABSTRACT

Periodontal regeneration is of utmost importance in the field of dentistry which essentially reconstitutes and replaces the lost tooth supporting structures. For this purpose, nano bioactive glass ceramic particle (nBGC) incorporated alginate composite scaffold was fabricated and characterized using SEM, EDAX, AFM, FTIR, XRD and other methods. The swelling ability, in vitro degradation, biomineralization and cytocompatibility of the scaffold were also evaluated. The results indicated reduced swelling and degradation and enhanced biomineralization and protein adsorption. In addition, the human periodontal ligament fibroblast (hPDLF) and osteosarcoma (MG-63) cells were viable, adhered and proliferated well on the alginate/bioglass composite scaffolds in comparison to the control alginate scaffolds. The presence of nBGC enhanced the alkaline phosphatase (ALP) activity of the hPDLF cells cultured on the composite scaffolds. Thus results suggest that these biocompatible composite scaffolds can be useful for periodontal tissue regeneration.

1. Introduction

Regeneration of damaged or missing tissues generally gets complicated as the structure gets more complex. Regeneration of lost tooth supporting structures is a highly orchestrated biological process involving a cellular and molecular interplay (Chen & Jin, 2010). The reparative potential of periodontium is extremely limited in adult teeth and hence only therapeutic intervention has the possibility to induce its regeneration so that the form and function of the lost structures are restored (Aichelmann-Reidy & Reynolds, 2008). It is commonly found that the epithelial tissues migrate rapidly into the wound, preventing periodontal regeneration (Nyman, Lindhe, Karring, & Rylander, 1982). To subjugate this, procedures such as Guided Tissue Regeneration (GTR), employ the placement of a barrier membrane to prevent early epithelial migration and wound closure. However these membranes do not regenerate the damaged tooth supporting tissues (Ivanovski, 2009). Conventional surgical procedures such as open flap debridement provide significant access to evaluate and detoxify root surfaces; however, these surgical techniques offer only limited potential in restoring or reconstituting component periodontal tissues (Reynolds, Aichelmann-Reidy, & Branch-Mays, 2010). Regenerative procedures frequently include bone grafting materials to encourage the growth of key surrounding tissues, while excluding unwanted cell types such as epithelial cells (Melcher, 1976). Autogenous bone graft materials have shown new connective tissue attachment only with the formation of long junctional epithelium. Xenograft and allograft materials too have not shown any enhanced improvement in gaining attachment by means of new connective tissue formation without the aid of GTR (Karring, Lindhe, & Cortellini, 1998). Thus biologic rationale for the regeneration of the periodontium is missing which is a fundamental problem pertaining to all bone fillers (Bosshardt & Sculean, 2009).

Scaffolds developed from natural and synthetic polymers are commonly used in tissue engineering. These polymers mimic the chemical and physical properties of natural extra cellular matrix (ECM) (Kim et al., 2011; Liu et al., 2008). Alginate is a natural polysaccharide extracted from brown seaweeds. Chemically, alginate is a linear polymeric acid composed of 1,4-linked β-D-mannuronic acid (M) and α-L-guluronic acid (G) residues. In the presence of certain divalent cations (e.g., Ca^{2+}, Sr^{2+} and Ba^{2+}) at low concentrations, alginate has the ability to form stable hydrogels through ionic interaction between the cation and the carboxyl functional group of G units located on the polymer chain (Wang, Zhang, Konno, & Saito, 1993). It is highly hydrophilic, biocompatible, relatively economical and widely utilized in the food and pharmaceutical industry. Due to their highly hydrophilic nature, seeding of cells onto the scaffolds is simple and rapid (Wang et al., 2003). Cross linking makes alginate insoluble in aqueous

* Corresponding author. Tel.: +91 484 2801234; fax: +91 484 2802020.
E-mail addresses: jayakumar77@yahoo.com, rjayakumar@aims.amrita.edu (R. Jayakumar).

0144-8617/$ – see front matter © 2011 Elsevier Ltd. All rights reserved.
doi:10.1016/j.carbpol.2011.07.058

solution and culture medium. This enables it to remain as supporting structure for the seeded cells when it is used as a scaffold both in vitro and in vivo. When used in vivo, ionically crosslinked alginate degrades when the calcium ions are exchanged with other ions in the body, such as Na^+ (Bonino et al., 2011; Mohan & Nair, 2005).

Bioglasses are the most preferred bioactive fillers that form a bond to both hard and soft tissues without an intervening fibrous tissue layer due to formation of carbonated apatite layer on their surface in physiological fluid compared to other bioactive ceramic materials such as hydroxyapatite (HA), calcium phosphates (Heinemann et al., 2007; Heinemann, Ehrlich, Knieb, & Hanke, 2007; Hench, Splinter, Allen, & Greenlee, 1972). Since the discovery of bioglass by L. Hench, they have been applied as bone fillers, bone repair materials and adjuvants in bone grafts due to their enhanced biocompatibility, osteoconductive and osteoinductive properties (Peter et al., 2009, 2010). Bioactive glass ceramics have been reported to influence osteoblastic cell differentiation with an increase in the level of differentiation markers like alkaline phosphatase (ALP), osteocalcin and osteopontin (Valerio et al., 2004). They also enhance osteogenesis through a direct control over genes that regulate cell cycle induction and progression towards a mature osteoblast phenotype (Hench, 2009). Bioglasses of high purity, homogeneity and surface area can be obtained by sol–gel technique, a low temperature synthesis method in comparison to the fusion method (Xia & Chang, 2007). The addition of nano bioactive glass ceramic particles into scaffold material not only improves the biomineralization capability of the composite scaffolds but also increases the stiffness of the scaffold material without compromising the mechanical strength (Ehrlich, Heinemann, et al., 2008; Ehrlich, Janussen, et al., 2008; Rezwan et al., 2006). Due to the release of soluble silicon from bioglass, it has a soft tissue bonding property (Cao & Hench, 1996). Bioglass is also osteostimulative, due to its ability to stimulate growth factor production in addition to osteoconductivity (Ehrlich, 2010; Ehrlich, Simon, et al., 2010). The addition nano bioglass in polymeric matrices has shown to increase surface adsorption of proteins (Misra et al., 2010). The direct chemical bonding between bioglass and the surrounding tissues probably prevents the ingress of bacteria. The modulus of elasticity of bioglass matches more closely the elasticity of the surrounding tissues, thus reducing the possible risk of bone resorption (Gheysen et al., 1983). Hence to evaluate the influence of nBGC on alginate hydrogel for periodontal tissue regeneration, alginate hydrogel/nBGC composite scaffold was fabricated and studied in detail.

2. Materials and methods

2.1. Materials

Sodium alginate, Calcium chloride anhydrous, tetraethyl orthosilicate (TEOS), calcium nitrate tetrahydrate ($Ca(NO_3)_2.4H_2O$), ammonium dibasic phosphate ($NH_4H_2PO_4$), poly ethylene glycol (PEG), minimum essential medium (MEM), paraformaldehyde, Triton X-100, bicinchoninic acid (BCA), cupric sulphate, sodium dodecyl sulphate (SDS), CHAPS, bovine serum albumin, alkaline phosphatase lyophilized, glycine buffer and PNPP (paranitro phenol phosphate) liquid substrate were purchased from Sigma–Aldrich. Glutaraldehyde and Hen Lysozyme were purchased from Fluka. DAPI, Alamar Blue, Trypsin–EDTA and fetal bovine serum (FBS) were obtained from Gibco, Invitrogen Corporation. MG-63 was obtained from NCCS, Pune, India. hPDLF and Fibroblast medium were purchased from Science Cell, USA. Nitric acid (HNO_3) and liquid ammonia were purchased from Finar chemicals and Qualigens Fine chemicals respectively.

2.2. Methods

2.2.1. Synthesis of nano bioactive glass ceramic particles (nBGC)

The procedure for the preparation of nBGC was reported in our previous works (Sowmya et al., 2011). For the preparation of nBGC, 7.8 g of TEOS and 12.5 g of $Ca(NO_3)_2{\cdot}4H_2O$ were dissolved in a mixture of distilled water and ethanol (120 ml:40 ml) and stirred at room temperature. TEOS undergoes hydrolysis and a transparent solution was obtained. The pH value of this solution was adjusted to 2 with dilute HNO_3. 1.98 g of $NH_4H_2PO_4$ was dissolved in 1500 ml of distilled water containing 15 g of PEG (20,000 MW) and the pH of the solution was adjusted to 10 with ammonium water. When TEOS was completely hydrolyzed in about 4 h, the TEOS–$Ca(NO_3)_2$ solution was dropped into $NH_4H_2PO_4$ solution under vigorous stirring and the reaction mixture aged for 24 h at room temperature to obtain a white gel precipitate. Finally, $CaO–SiO_2–P_2O_5$ ternary BGC nanoparticles were obtained by filtration, lyophilisation (CHRIST ALPHA 2-4 LD Plus) and calcination of the precipitate.

2.2.2. Fabrication of alginate/nBGC composite scaffolds

3% sodium alginate gel was prepared by dissolving sodium alginate powder in distilled water and kept for overnight stirring. To the required weighed quantity of the above-prepared alginate gel, 0.5 and 1% of nBGC was added and stirred well until completely dissolved. The mixed alginate/nBGC gel was then transferred to a 24-well plate, pre-freezed at −20 °C for 12 h followed by lyophilization at −80 °C to obtain alginate/nBGC composite scaffolds. Fig. 1A and B shows the steps involved in the fabrication of composite scaffolds.

2.3. Characterization

The structural morphology of the composite scaffolds was examined using Scanning electron microscope (SEM) (JEOL, JSM-6490LA, Japan). Composite scaffold samples were prepared by taking thin sections with a razor blade. The sections were platinum sputtered in vacuum (JEOL, JFC-1600, Japan) and examined using SEM. FT-IR spectra of composite scaffolds, alginate (control) and nBGC were characterized using a FTIR spectrometer (Perkin-Elmer RX1). Dried composite scaffolds were ground and mixed thoroughly with potassium bromide at a ratio of 1:5 (Sample: KBr). The IR spectra were analyzed in the range of 400–4000 cm^{-1}. XRD pattern of the composites scaffolds, alginate (control) and nBGC were obtained at room temperature using a Panalytical (XPERT PRO powder diffractometer) (Cu Ka radiation) operating at a voltage of 40 kV. XRD was taken at 2θ angle range of 5–60° and the process parameters were: scan step size 0.02 (2θ) and scan step time 0.05 s. Thermogravimetric analysis of the composite scaffolds and alginate (control) was carried out using TG/DTA instrument (SII TG-DTA6200) at a temperature range of 25–500 °C.

2.4. Swelling studies

The swelling ability of the scaffolds was studied using in phosphate buffered saline (PBS) (pH 7.4) at 37 °C (Liuyun et al., 2009). The dry weight of the samples, i.e. alginate scaffold (control), alginate/0.5% and alginate/1% nBGC composite scaffolds were noted as W_d. The scaffolds were immersed in PBS solution (pH 7.4) at 37 °C for different time durations such as 1, 3 and 7 days respectively. After the predetermined time, the scaffolds were removed, the water absorbed on to the surface was gently blotted onto a filter paper and wet weight was recorded as W_w. The ratio of swelling was determined using Eq. (1):

$$\text{Swelling ratio} = \frac{W_w - W_d}{W_d} \quad (1)$$

Swelling ratio was expressed as mean ± SD ($n = 3$).

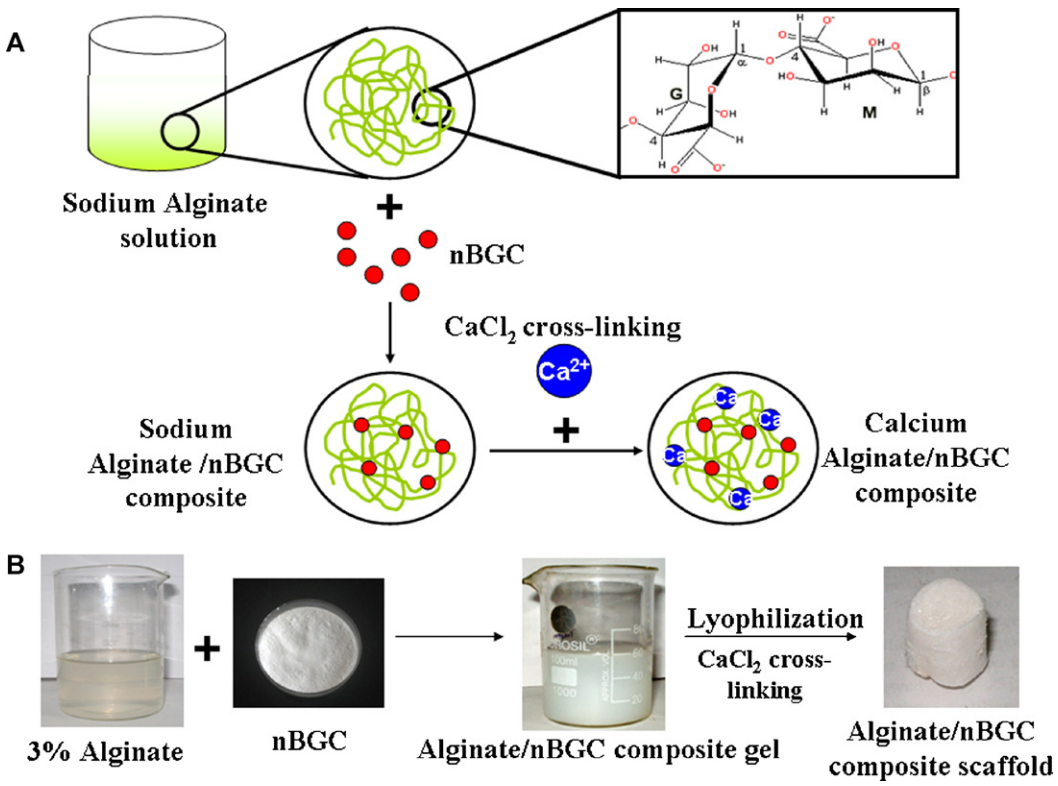

Fig. 1. (A) Schematic representation and (B) Laboratory fabrication of alginate/nBGC composite scaffold.

2.5. Porosity estimation

Liquid displacement method was used to determine the porosity of the scaffolds (Liuyun et al., 2009). Three samples each of alginate scaffold (control), alginate/0.5% nBGC and alginate/1% nBGC composite scaffolds were immersed in distilled water for 48 h until it gets fully saturated and the porosity of the sample was determined using Eq. (2)

$$P = \frac{W_2 - W_1}{\rho V_1} \quad (2)$$

where W_1 and W_2 represent the weight of the scaffolds before and after immersing in distilled water, V_1 is the volume of scaffold before immersing and ρ is a constant of the density of water.

Porosity was expressed as mean ± SD ($n = 3$).

2.6. In vitro degradation studies

The degradation of the scaffold was studied in PBS (pH 7.4) containing lysozyme at 37 °C (Peter et al., 2010). Three samples each of alginate scaffold (control), alginate/0.5% and alginate/1% nBGC composite scaffolds were immersed in lysozyme (10,000 U/ml) containing medium and incubated at 37 °C for 7, 14, 21 and 28 days, respectively. Initial weight of the scaffolds was noted (W_i). After soaking for 7, 14, 21 and 28 days, the scaffolds were removed from the solution and rinsed with deionised water to remove the adsorbed ions on the surface and freeze dried. The dry weight after lyophilisation was noted (W_t). The degradation of scaffold was calculated using Eq. (3):

$$\text{Degradation (rate of weight loss \%)} = \frac{W_i - W_t}{W_i} \times 100\% \quad (3)$$

Degradation rate was recorded as mean ± SD ($n = 3$).

2.7. Protein adsorption studies

Scaffolds of equal shape and weight were placed in 96-well plate containing minimum essential media (MEM) + 10% FBS and incubate at 37 °C for specified time duration (30 min, 1, 2, 4 and 6 h). After the specified incubation, the scaffolds were rinsed with PBS solution thrice. The rinsed scaffolds were then incubated with the elution buffer for 1 h at 37 °C. Total protein was quantified using bicinchoninic acid (BCA) assay (Hulbert et al., 1970; Walker, 1994). The principle of BCA assay is based on the reduction of Cu^{2+} to Cu^{1+}. The amount of reduction is proportional to the protein present. BCA reagent was added to each well and incubated for 30 min with the extract at 37 °C and the absorbance was read at a wavelength of 562 nm. Scaffolds incubated in serum free medium were used as blank (Binulal et al., 2010). The protein adsorption was calculated as mean ± SD ($n = 3$).

2.8. In vitro biomineralization studies

Alginate scaffold (control), alginate/0.5% and alginate/1% nBGC composite scaffolds of equal weight and shape were immersed in 1× simulated body fluid (SBF) prepared (Kokubo & Takadama, 2006) by adding NaCl (7.995 g), KCl (0.224 g), $CaCl_2 \cdot 2H_2O$ (0.368 g), $MgCl_2 \cdot 6H_2O$ (0.305 g), K_2HPO_4 (0.174 g), $NaHCO_3$ (0.349 g) and $Na_2SO_4 \cdot 10H_2O$ (0.161 g) to 1 L of distilled water. The pH of the solution was adjusted to 7.4 by the addition of Tris/HCl. The samples immersed in SBF were kept for incubation at 37 °C in closed falcon tubes for 7, 14, 21 and 28 days. After the precise time duration, the scaffolds were removed, washed with deionised water to remove the adsorbed minerals, lyophilized, sectioned and viewed using SEM and EDAX for mineralization. The formation of minerals was also confirmed by analyzing the XRD spectra of the SBF mineralized scaffolds ($n = 3$).

2.9. Cell viability studies

Cell viability of the alginate scaffold (control), alginate/0.5% and alginate/1% nBGC composite scaffolds was evaluated by direct cell viability using Alamar Blue assay (Binulal et al., 2010). Alamar blue reagent is a cell viability and cell proliferation indicator that uses the inherent reducing power of live cells as an indicator of metabolic activity. It works through the conversion of resazurin to resorufin. Resazurin, a nonfluorescent indicator dye, is converted to highly red-fluorescent resorufin via redox reactions in metabolically active cells. The magnitude of the fluorescence signal is proportional to the number of living cells. Triplicates of each sample of equal weights were taken and sterilized using ethylene oxide gas (EtO). MG-63 cells have been proven to proliferate on bioactive glass surface. Though these osteosarcoma cells possess abnormal growth characteristics, they initially represent clonal populations derived from specific stages of the osteoblast lineage. MG-63 cells are considered to show a number of features typical of an undifferentiated osteoblast phenotype. This includes the synthesis of collagen types I and III, expression of alkaline phosphatase and production of osteocalcin. Due to these advantages offered by the MG-63 cells, they have been chosen to evaluate their role in alveolar bone regeneration, a periodontal tissue (Clover & Gowen, 1994; Price et al., 1997). Human osteosarcoma cells (MG63) and hPDLF cells cultured in MEM supplemented with 10% FBS, 50 IU ml^{-1} penicillin and 50 μg ml^{-1} streptomycin (Invitrogen, CA, USA) and fibroblast medium (Science Cell, California, USA) were seeded onto a 96-well plate at a density of 1×10^4 cells/well and incubated at 37 °C for 48 h respectively. After the incubation period of 48 h, the media was replaced with 100 μl of fresh media containing 10% of Alamar blue solution. After 4 h of incubation, the scaffold samples were removed and the OD of the solution was measured at a wavelength of 570 and 600 nm using a Microplate reader (Biotek PowerWave XS, USA).

2.10. Alkaline phosphatase activity

Pre-weighed scaffolds of alginate scaffold (control), alginate/0.5% and alginate/1% nBGC composite scaffolds washed with PBS were placed in a 24-well plate and hPDLF cells (8000 cells/scaffold) were seeded onto the scaffolds and incubated at 37 °C in a humidified incubator with 5% CO_2 and 85% humidity for different time intervals of 7, 14, 21 and 28 days. After 4 h cells were fed with additional periodontal cell specific growth medium. At the pre-determined time interval, the scaffolds were removed, washed with PBS and incubated with 1% Triton X-100 for 2 h to obtain cell lysates. The cell lysates were ultrasonicated for 30 min and aliquots of the supernatant were incubated with p-nitrophenylphosphate in the presence of glycine buffer for 30 min. The ALP activity of the cells was determined by a spectrophotometric endpoint assay that determines the conversion of colourless p-nitrophenyl phosphate substrate into coloured p-nitrophenol. The phosphatase activity is proportional to the production of p-nitrophenol. The reaction was stopped by adding 5 M NaOH. Sample absorbance was measured at 405 and 490 nm. Standards were prepared from p-nitrophenol. The alkaline phosphatase activity was calculated as mean ± SD ($n = 3$).

2.11. Cell attachment and proliferation studies

Cell attachment and proliferation studies of alginate scaffold (control), alginate/0.5% and alginate/1% nBGC composite scaffolds were conducted using MG-63 and hPDLF cells cultured in MEM supplemented with 10% FBS and 100 U/ml penicillin–streptomycin and fibroblast media respectively. Prior to cell seeding, scaffolds were sterilized using EtO and incubated with culture medium for 1 h at 37 °C in a humidified incubator with 5% CO_2 and 85% humidity. After the incubation period, the culture medium was removed completely from the scaffolds. Cells were seeded drop wise onto the top of the scaffolds (1×10^5 cells/scaffold), which fully absorbed the media, allowing the cells to distribute throughout the scaffolds. Consequently, the cell-seeded scaffolds were kept at 37 °C in a humidified incubator for 12 and 72 h to allow the cells to attach and proliferate throughout the scaffolds. After 4 h, the scaffolds were fed with additional culture medium. After 12 and 72 h of incubation, the scaffolds for SEM analysis were washed with PBS and fixed with 2.5% glutaraldehyde for 1 h following which the scaffolds were thoroughly washed with PBS and sequentially dehydrated in a graded ethanol series, air-dried, platinum sputtered in vacuum and examined.

For DAPI staining, the scaffolds were fixed with 4% paraformaldehyde in PBS for 20 min. Following this the scaffolds were washed with PBS and permeabilised with 0.5% Triton X-100 (in PBS) for exactly 5 min. The scaffolds were blocked using 1% FBS (in PBS), washed with PBS, stained with 50 μl DAPI (in PBS) and incubated in dark for 5 min. The scaffolds were then thoroughly washed with PBS and viewed under fluorescent microscope (Olympus-BX-51).

2.12. Statistical analysis

All quantitative results were obtained from triplicate samples. Data was expressed as the mean ± SD. Statistical analysis was carried out using Student's two-tailed t-test. A value of $p < 0.05$ was considered to be statistically significant.

3. Results and discussion

3.1. Characterization of nBGC and composite scaffolds

Fig. 2 shows the SEM image of alginate control (A) and alginate/nBGC composite scaffold (B), indicating the porous nature of the composite scaffolds. The size of the pores decreased with the addition of the nBGC. The pore size was found to be in the range of 100–300 μm suitable for tissue engineering applications (Karageorgiou & Kaplan, 2005). Pores are essential for the migration and proliferation of the cells, nutrient supply and vascularisation (Peter et al., 2010; Sowmya et al., 2011). The surface of the alginate control scaffold was found to be smooth compared to the alginate/nBGC composite scaffold. This could be due to the incorporation of nBGC that significantly increases the surface area of the scaffolds further enhancing the bioactivity of the scaffolds (Boccaccini et al., 2010).

Fig. 2C shows the FTIR spectra. FTIR spectra of nBGC showed vibration bands at 467 cm^{-1} and a shoulder at 1200 cm^{-1} which are assigned to Si–O–Si bending mode (Heinemann, Ehrlich et al., 2007; Ehrlich et al., in press). The vibration band at 1070 cm^{-1} and a double peak at 607 and 567 cm^{-1} are due to the stretching vibration of phosphate groups (Ehrlich et al., 2010; Madhumathi et al., 2009a,b; Sowmya et al., 2011; Xia & Chang, 2007). The peaks at 2889 and 1637 cm^{-1} are attributed to CH stretching and O–H (molecular water) bending vibration band of PEG. This indicates that PEG is present on the surface of nBGC (Tan & Kacey, 2010). FT-IR spectra of alginate scaffold showed an intense peak around 3420 cm^{-1} indicates the absorption of O–H group. A peak around 1400–1444 cm^{-1} is due to the presence of carboxyl group. Peaks at 1630 and 1000–1240 cm^{-1} ascertain to the presence of carbonyl groups. In particular the peaks at 1000–1125 and 1240 cm^{-1} region confirmed the presence of guluronic acid, mannuronic acid and o-acetyl ester, the building blocks of alginic acid (Kazy et al., 2002). For alginate/nBGC composite scaffolds FTIR spectra showed the combined peaks of alginate and nBGC which confirmed the incorporation of nBGC into the alginate scaffold.

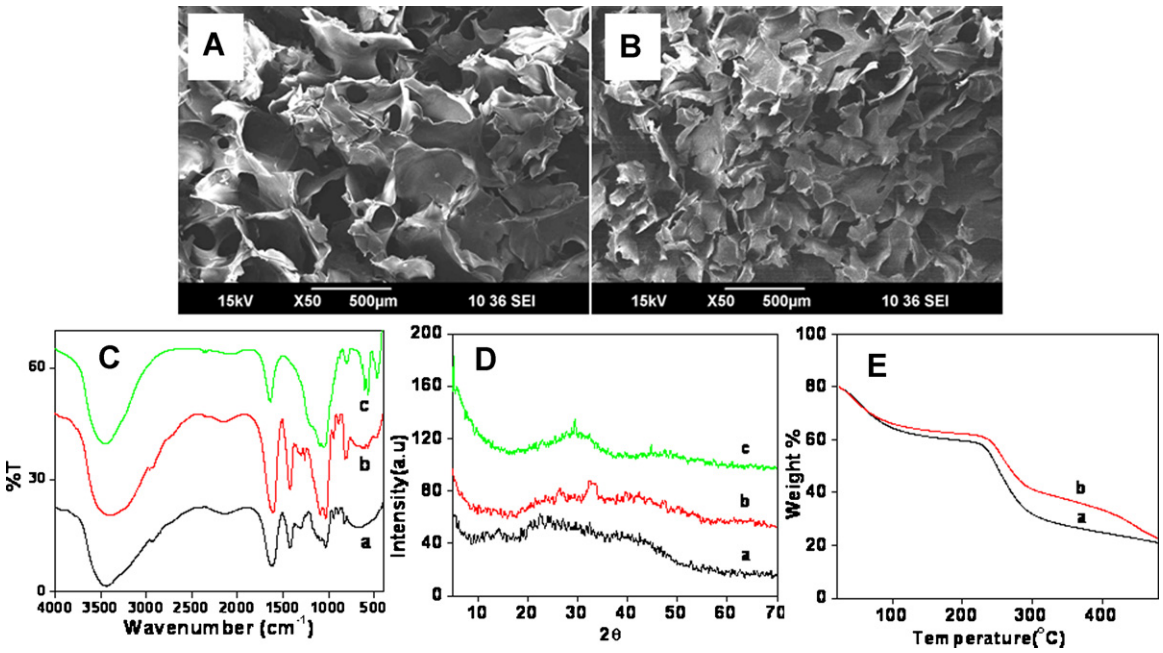

Fig. 2. SEM images showing macroporous structure of A() alginate scaffold and (B) alginate/nBGC composite scaffold, with pore size ranging from 100 to 300 μm. (C) FT-IR spectra of (a) alginate scaffold (control), (b) alginate/nBGC composite scaffold, (c) nBGC. (D) XRD spectra of (a) alginate scaffold (control), (b) alginate/nBGC composite scaffold, (c) nBGC. (E) TGA profile of (a) alginate scaffold (control) and (b) alginate/nBGC composite scaffold.

Fig. 2D shows the XRD spectrum of the prepared nBGC and scaffolds. The XRD spectra of nBGC confirmed that they generally exist in amorphous state. There are no diffraction peaks except a broad band between 20 and 40° (2θ) (Xia & Chang, 2007). The XRD spectrum of alginate also indicates a broad peak between 20 and 50° (2θ). Thus, the XRD spectra of the alginate/nBGC composite scaffolds also were amorphous in nature with a peak at 32° (2θ) specific to the low intensity crystalline nature of nBGC.

Fig. 2E shows the TGA profile. TGA illustrated that all the scaffolds showed decomposition in the range of 50–100 °C due to loss of moisture content from the scaffolds. A second decomposition was seen in the range of 220 to 280 °C for alginate control scaffold and 230–290 °C for the alginate/nBGC composite scaffolds. This is attributed to the decomposition of the polysaccharide structure of alginate. The presence of nBGC decreased the rate of decomposition of alginate/nBGC composite scaffold in comparison to the alginate control scaffold (Sowmya et al., 2011).

3.2. Swelling studies

The swelling behaviour of the alginate control scaffolds and alginate/nBGC composite scaffolds are shown in Fig. 3A. nBGC

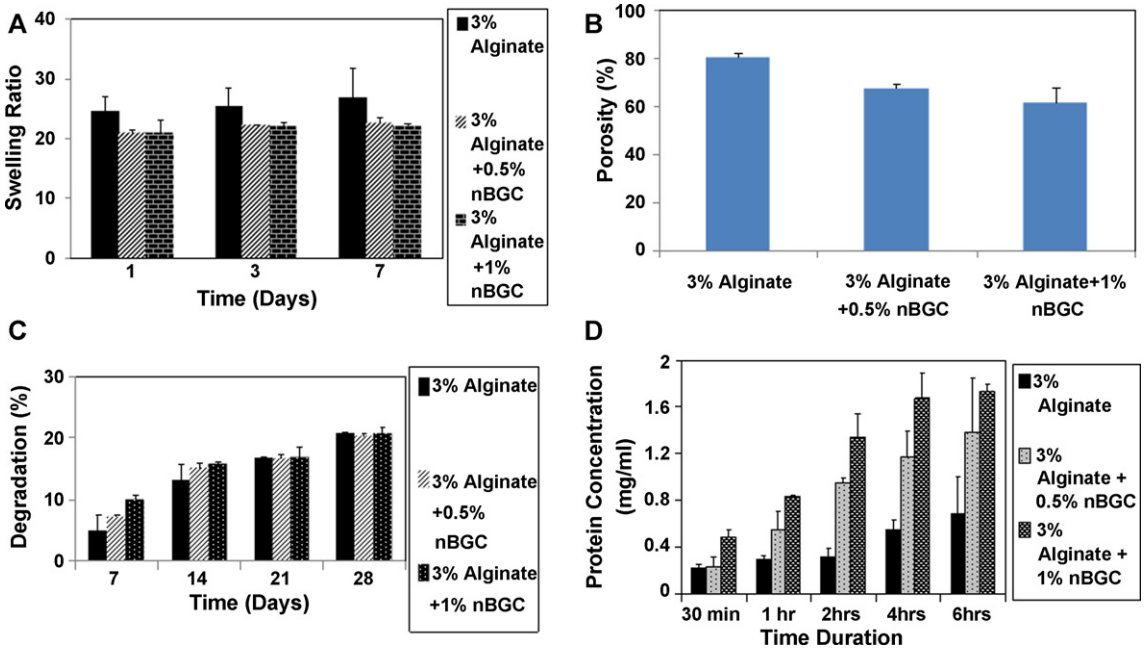

Fig. 3. (A) Swelling studies of alginate scaffolds in PBS. (B) Porosity studies of alginate scaffolds. (C) In vitro degradation profile of alginate scaffolds in PBS–lysozyme. (D) Protein adsorption studies of alginate scaffolds.

incorporated scaffolds showed lower swelling percentage compared to the control scaffolds. This may be due to the strong interaction between alginate and nBGC. This may also be attributed to the reduction in the pore size with the addition of nBGC. The swelling was found to increase with time until day 7, following which the scaffolds slowly started degrading. Swelling and porosity aid in the supply of nutrients to the interior of the composite scaffolds and also increase the surface area for the cells to adhere that is essential for tissue engineering scaffolds. But increased swelling affects the mechanical property of the material, thus a controlled swelling is appreciated for any tissue engineering application (Peter et al., 2009, 2010).

3.3. Porosity studies

The porosity of the alginate control scaffolds and alginate/nBGC composite scaffolds are shown in Fig. 3B. With the increase in the concentration of nBGC, the percentage of porosity was found to decrease. Porosity is essential for the transport of oxygen and nutrients to the interior of the scaffolds. A reduction in porosity percentage of the composite scaffolds was observed, but this controlled porosity is satisfactorily favourable for tissue engineering applications (Karageorgiou & Kaplan, 2005). The presence of bioglass in the composite scaffold supports tissue in-growth. Porosity offered by the composite scaffold enhances the bone bonding ability due to the following reasons: (a) high surface area to volume ratio offered by nanobioglass has the tendency to bioresorb and induce bioactivity, (b) interconnected pores can provide a framework for bone growth into the matrix of the implant, and thus anchor them with the surrounding bone, preventing micro-motion that in turn increases further bone growth, (c) interconnected porosity is also a source of nutrient supply, vascularization and waste removal (Nandi, Kundu, Datta, De, Basu, 2009).

3.4. In vitro degradation studies

The in vitro degradation profile of alginate control and alginate/nBGC composite scaffolds is shown in Fig. 3C. Initially until day 14, the degradation of the composite scaffolds was slightly increased when compared to the control scaffolds. This may be due to the preferential dissolution of inorganic component from the nBGC particles during incubation (Hong et al., 2008). After day 21, the rate of degradation of the composite scaffolds was comparable/slightly lesser in comparison to the alginate control scaffolds. The control and composite scaffolds lost about 21% of their weight after 28 days of incubation with lysozyme. The 1–4 glycosidic linkages of alginate are susceptible to degradation by lysozyme due to the ionic interaction of the negatively charged alginate with lysozyme. This results in the formation of simple glucose type residues (Hunt et al., 2010). The degradation rate of alginate is drastically reduced due to the presence of nBGC and ionic cross-linking with calcium ions. The divalent calcium ions dissipate as a result of exposure to monovalent cations such as sodium, potassium and phosphate ions present in the media containing lysozyme (Mohan & Nair, 2005). The leachable alkaline products of nBGC neutralize the degradation products of alginate thus reducing the degradation rate of the scaffold (Sowmya et al., 2011). An ideal tissue engineering scaffold should be biodegradable and the rate of degradation should match the rate of tissue regeneration (Roman et al., 2003). The result shows that the composite scaffolds are biodegradable thus, satisfying the ideal requirements of a tissue engineering scaffold.

3.5. Protein adsorption studies

Fig. 3D indicates the protein adsorption data of the scaffolds. The protein adsorption studies showed significant increase in the protein adsorption in the alginate/nBGC composite scaffolds compared to the alginate control scaffold with the increase in time duration. It also increased with the increase in the percentage of nBGC. Protein adsorption is known to influence cell adhesion by adsorption of key adhesion molecules like fibronectin or vitronectin (Binulal et al., 2010; Sudheesh et al., 2011). The increase in protein adsorption on the nano-composite scaffolds could be due to the exposed nBGC on the scaffold surfaces, which increases the binding sites on the material surface and more total surface area for proteins or promotes an electrostatic interaction between the proteins and material surface thus enhancing adsorption of proteins (Hunt et al., 2010). The interaction between protein and bioglass is facilitated primarily by hydrogen bonds and electrostatic bonds. Electrostatic interaction occurs between the negatively charged silica surface (dissociated silanols) and protonated amine groups (–NH:) of proteins, and this interaction is generally irreversible. The formation of a silica-rich gel layer due to ion exchange provides a suitable substrate for extracellular adsorption, particularly of nonsteroid hormones, growth factors and attachment factors. It is the highly hydrolyzed, porous nature and high surface charge density of the silica surface of bioglass that induces strong protein adsorption (Lobel & Hench, 1996). Further studies are needed to find out the specific protein adsorbed on the scaffold surface and their role in cell attachment and behaviour on the nano-composite scaffold.

3.6. In vitro biomineralization with respect to formation of HA

Fig. 4A–D shows the SEM images of in vitro biomineralization studies of the scaffolds. The in vitro biomineralization of the alginate control and alginate/nBGC composite scaffolds immersed in 1× SBF for 7, 14, 21 and 28 days were analysed. The SEM images showed an apatite rich layer deposition on the surface of the scaffolds that was more pronounced in the alginate/nBGC composite scaffolds than the control scaffolds. The deposition of HA increased exponentially from 7 to 21 days.

Fig. 4E shows the XRD spectra of biomineralized scaffolds. The XRD spectra of alginate/nBGC composite scaffolds showed sharp peaks 31.8 and 46.7° (2θ) attributed to 211 and 222 plane of HA (Chai et al., 1995; Tan & Kacey, 2010). The increase in the intensity of peaks from day 7 to 28 was indicative of increase in the deposition of HA. It also confirmed that the presence of nBGC has increased the deposition of HA on the scaffolds (Kokubo et al., 2003). EDS spectra of the mineralization of alginate/nBGC composite scaffolds is shown in Fig. 4F, indicating a Ca:P ratio of 1.7 in comparison to the alginate control which is approximately close to the normal Ca:P ratio of 1.67. These results confirmed the bioactive nature of the composite scaffolds and hence may be ideal for cell and extracellular matrix deposition of bone composed of inorganic apatite essential for dental and orthopaedic appliances.

3.7. Cell viability studies

Cytocompatability of the alginate control and alginate/nBGC composite scaffolds was assessed using alamar blue assay with hPDLF and MG-63 cells shown in Fig. 5A and B. The OD value of the alginate/nBGC nanocomposite scaffolds does not show any significant decrease when compared to the positive control (cells incubated in media alone) after 48 h. The nBGC can cause alkalization of culture medium due to the leachable products from nBGC, which may lead to an increase in Ca^{2+} ions in culture medium thereby inducing apoptosis of the cells (Roman et al., 2003).

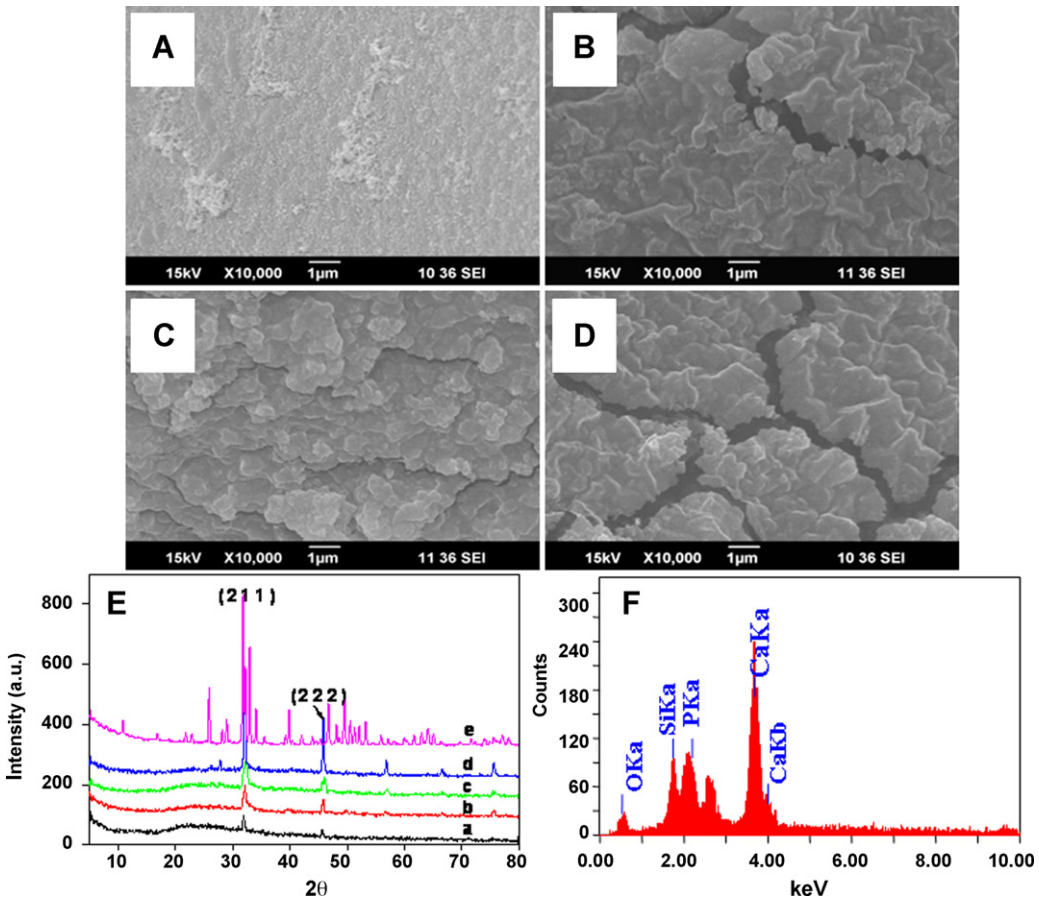

Fig. 4. SEM images of in vitro biomineralization of (A) alginate (control) scaffold in SBF after 21 days and alginate/nBGC composite scaffold in SBF after (B) 7, (C) 14 and (D) 21 days. (E) XRD spectra of in vitro biomineralization in SBF (a) alginate (control) scaffold after 21 days and alginate/nBGC composite scaffold after (b) 7, (c) 14 and (d) 21 days and (e) HA. (F) EDS spectra of in vitro biomineralization in SBF of alginate/nBGC composite scaffold after 21 days.

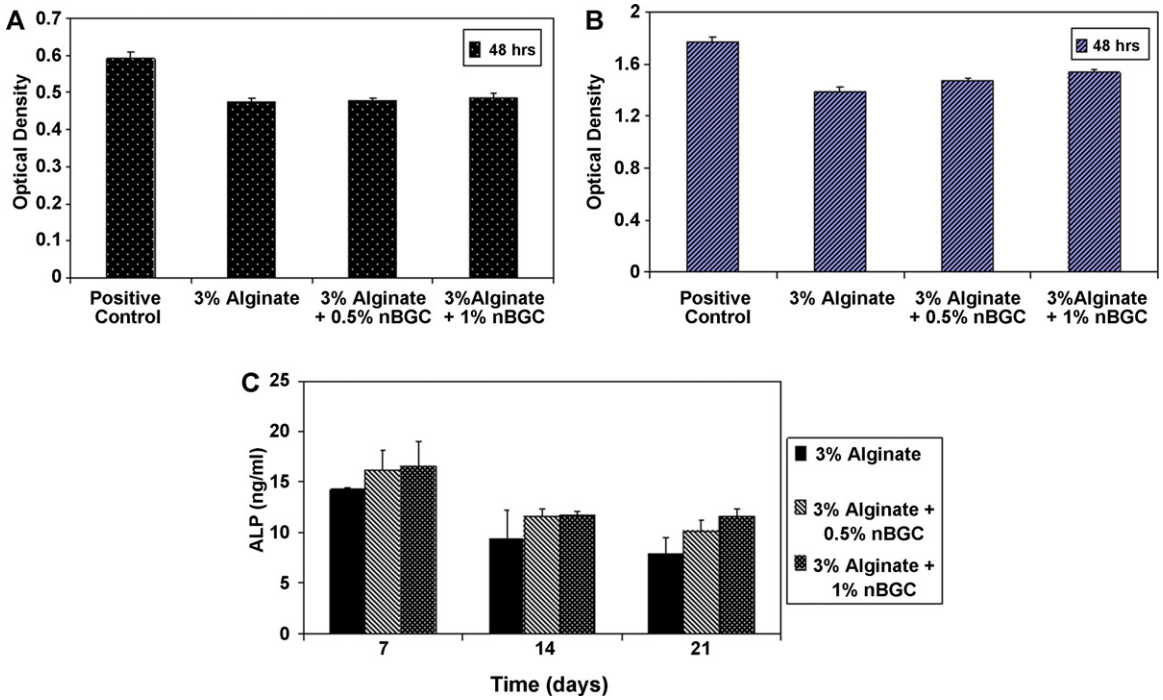

Fig. 5. (A) Cell viability of alginate scaffold and alginate/nBGC composite scaffold for hPDLF cells using Alamar Blue assay (positive control-media + cells). (B) Cell viability of alginate scaffold and alginate/nBGC composite scaffold for MG-63 cells using Alamar Blue assay (positive control-media + cells). (C) ALP activity of alginate (control) and alginate/nBGC composite scaffolds.

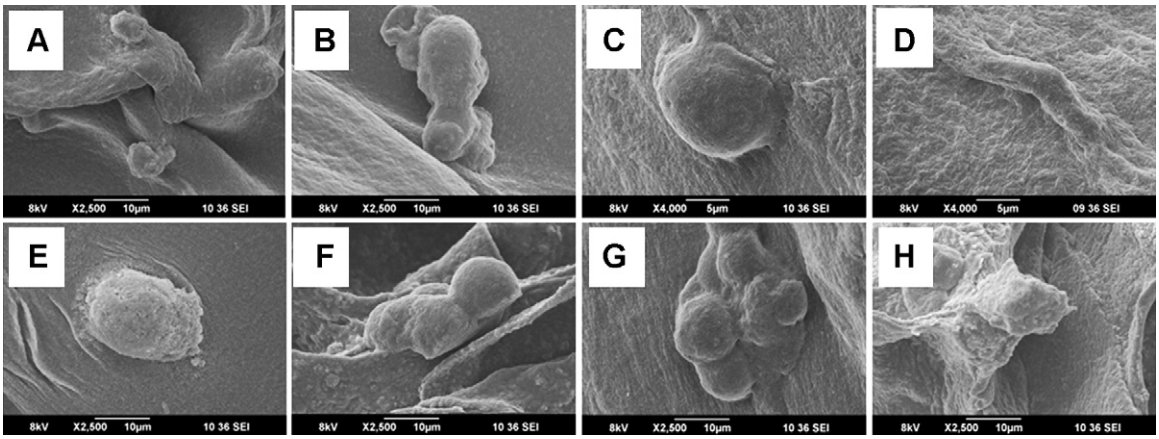

Fig. 6. SEM images of cell attachment (12 h) of hPDLF cells on (A) alginate (control), (B) alginate/nBGC composite scaffold. SEM images of hPDLF cell spreading (proliferation 72 h) of hPDLF cells on (C) alginate (control), (D) alginate/nBGC composite scaffold. SEM images of cell attachment (12 h) of MG-63 cells on (E) alginate (control), (F) alginate/nBGC composite scaffold. SEM images of cell spreading (proliferation 72 h) of MG-63 cells on (G) alginate (control), (H) alginate/nBGC composite scaffold.

However, the results indicated that there is no significant reduction in cell viability compared to the positive control demonstrating that composite scaffolds are biocompatible.

3.8. Alkaline phosphatase activity

Fig. 5C shows the ALP activity of the alginate control and alginate/nBGC composite scaffolds. ALP is an important early osteogenic differentiation and biochemical marker of osteoblasts. Studies have indicated that PDL cells exhibit ALP activity and thus also behave as osteoblasts (Basdra & Komposch, 1997). ALP activity of hPDLF cells cultured on alginate/nBGC composite scaffolds was maximal at 7 days followed by a decline in its activity thereafter. Earlier studies have reported a decrease in ALP activity after prolonged incubation (Donzelli et al., 2007). The initial increase in ALP activity up to 7th day indicates the completion of osteoblastic differentiation followed by a decrease during 14 and 21 days that correlates to the maturation of the PDLF cells and advanced matrix mineralization (Donzelli et al., 2007). The ALP activity of alginate scaffolds has already been proved earlier and hence their application for bone tissue engineering. However, the presence of bioglass in the composite scaffold further enhances the ALP activity in comparison to the control alginate scaffold. This could be due to the release of ions and dissolution products from the bioactive glass that activate and up-regulate gene expression in osteoprogenitor cells that give rise to rapid bone regeneration. Also the presence of silicon in bioglass is known to be a stimulating factor in osteoblast ALP production (Andrade et al., 2006; Xynos et al., 2000). Thus the results confirmed the osteoblast-like behaviour of hPDLFs showing ALP activity.

3.9. Cell attachment and proliferation studies

The cell attachment and proliferation of MG-63 and hPDLF cells on alginate/nBGC composite scaffolds were studied using the SEM micrographs shown in Fig. 6 and DAPI stained fluorescent images shown in Fig. 7. SEM images revealed that cells adhered to the surface of the composite scaffolds and retained their characteristic morphology after incubation in comparison to the control alginate scaffolds. Within 72 h of incubation, the cells of rounded morphology further flattened and spread evenly throughout the surface of the scaffolds. The enhanced attachment and proliferation may be due to the increase in the surface area and surface roughness in the composite scaffold due to the incorporation of nBGC. SEM images also indicated the formation of bridges between the pores of the scaffolds by the cells. The fluorescent images of DAPI staining also showed enhanced attachment and proliferation of cells on the composite scaffolds in comparison to the alginate control scaffolds.

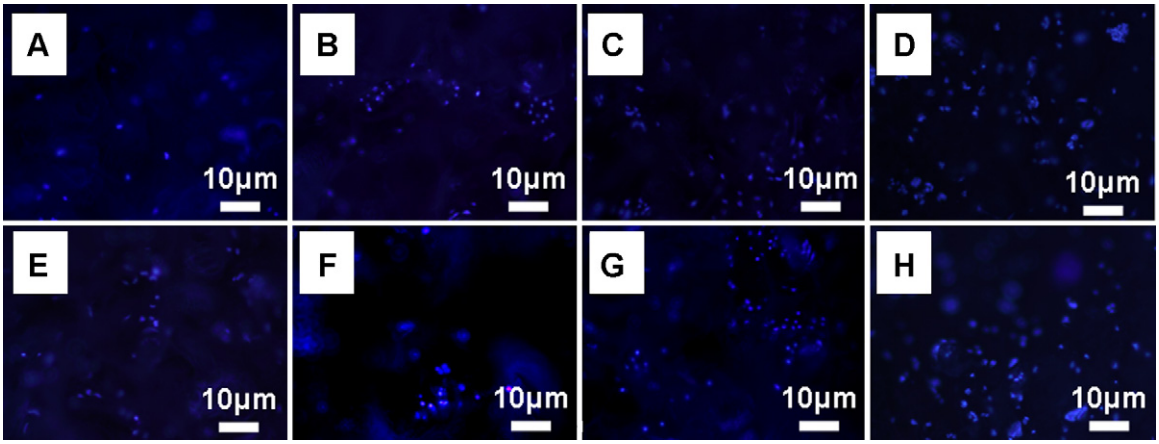

Fig. 7. Fluorescent images of DAPI staining of cell attachment of hPDLF cells (12 h) on (A) alginate (control), (B) alginate/nBGC composite scaffold. Fluorescent images of DAPI staining of cell proliferation (72 h) of hPDLF cells on (C) alginate (control), (D) alginate/nBGC composite scaffold. Fluorescent images of DAPI staining of cell attachment (12 h) of MG-63 cells on (E) alginate (control), (F) alginate/nBGC composite scaffold. Fluorescent images of DAPI staining of cell proliferation (72 h) of MG-63 cells on (G) alginate (control), (H) alginate/nBGC composite scaffold.

4. Conclusions

Alginate/nBGC composite scaffolds were successfully fabricated using lyophilization technique and characterized. The scaffolds were found to have characteristic materialistic and biological properties essential to facilitate periodontal regeneration. The composite scaffolds had a pore size of about 100–300 μm, controlled porosity and swelling ability, limited degradation and enhanced biomineralization, ideally controlled due to the presence of nBGC in the alginate scaffold. Incorporation of nBGC did not alter the viability of MG-63 and hPDLF cells and also helped to attain good protein adsorption, cell attachment and cell proliferation onto the scaffolds. The hPDLF cells also showed distinct osteoblast-like behaviour with enhanced alkaline phosphatase activity. All these results suggested that alginate/nBGC composite scaffold can serve as an appropriate bioactive matrix for periodontal tissue regeneration, thus indicating signs of another successive outbreak in the field of periodontal tissue engineering.

Acknowledgements

One of the authors R. Jayakumar is grateful to Department of Biotechnology (DBT), India, for providing the fund under the scheme of Nanoscience and Nanotechnology Program (Ref. No. BT/PR13585/NNT/28/474/2010). The author R. Jayakumar is also grateful to SERC Division, Department of Science and Technology (DST), India, for providing the fund under the scheme of Fast Track Scheme for Young Investigators (Ref. No. SR/FT/CS-005/2008). The authors are also grateful to Nanomission, DST, India, which partially supported this work, under the Nanoscience and Nanotechnology Initiative program monitored by Dr. C.N.R. Rao. The authors are also thankful to Mr. Sajin P. Ravi for his help in SEM studies.

References

Aichelmann-Reidy, M. E., & Reynolds, M. A. (2008). Predictability of clinical outcomes following regenerative therapy in intrabony defects. *Journal of Periodontology*, *79*, 387–393.

Andrade, A. L., Valerio, P., Goes, A. M., Leite, M. F., & Domingues, R. Z. (2006). Influence of morphology on in vitro compatibility of bioactive glasses. *Journal of Non-Crystalline Solids*, *352*, 3508–3511.

Basdra, E. K., & Komposch, G. (1997). Osteoblast-like properties of human periodontal ligament cells: an in vitro analysis. *European Journal of Orthodontics*, *19*, 615–621.

Binulal, N. S., Deepthy, M., Selvamurugan, N., Shalumon, K. T., Suja, S., Mony, U., et al. (2010). Role of nanofibrous poly(caprolactone) scaffolds in human mesenchymal stem cell attachment and spreading for in bone tissue engineering-response to osteogenic regulators. *Tissue Engineering: Part A*, *16*, 393–404.

Boccaccini, A. R., Erol, M., Stark, W. J., Mohn, D., Hong, Z., & Mano, J. F. (2010). Polymer/bioactive glass nanocomposites for biomedical applications: A review. *Composites Science and Technology*, *70*(13), 1764–1776.

Bonino, C. A., Krebs, M. D., Saquing, C. D., Jeong, S. I., Shearer, K. L., Alsberg, E., et al. (2011). Electrospinning alginate-based nanofibers: from blends to crosslinked low molecular weight alginate-only systems. *Carbohydrate Polymers*, *85*, 111–119.

Bosshardt, D. D., & Sculean, A. (2009). Does periodontal tissue regeneration really work? *Periodontology 2000*, *51*, 208–219.

Cao, W., & Hench, L. L. (1996). Bioactive materials. *Ceramics International*, *22*, 493–507.

Chai, C., Nissan, B. B., Pyke, S., & Evans, L. (1995). Sol-gel derived hydroxylapatite coatings for biomedical applications. *Materials and Manufacturing Processes*, *10*, 205–216.

Chen, F. M., & Jin, Y. (2010). Periodontal tissue engineering and regeneration: current approaches and expanding opportunities. *Tissue Engineering Part B: Reviews*, *16*, 219–255.

Clover, J., & Gowen, M. (1994). Are MG-63 and HOS TE85 human osteosarcoma cell lines representative models of the osteoblastic phenotype? *Bone*, *15*, 585–591.

Donzelli, E., Salvade, A., Mimo, P., Vigano, M., Morrone, M., Papagna, R., et al. (2007). Mesenchymal stem cells cultured on a collagen scaffold: in vitro osteogenic differentiation. *Archives of Oral Biology*, *52*, 64–73.

Ehrlich, H. (2010). *Biominerals, biological materials of marine origin invertebrates*. Dordrecht: Springer Verlag. (Part I) p. 569.

Ehrlich, H., Heinemann, S., Heinemann, C., Simon, P., Bazhenov, V. V., Shapkin, N. P., et al. (2008). Nanostructural organization of naturally occurring composites. Part I. Silica–collagen-based biocomposites. *Journal of Nanomaterials*, doi:10.1155/2008/623838. Article ID 623838

Ehrlich, H., Janussen, D., Simon, P., Bazhenov, V. V., Shapkin, N. P., Erler, C., et al. (2008). Nanostructural organization of naturally occurring composites. Part II. Silica–chitin-based biocomposites. *Journal of Nanomaterials*, doi:10.1155/2008/670235. Article ID 670235

Ehrlich, H., Simon, P., Carrillo-Cabrera, W., Bazhenov, V. V., Botting, J. P., Ilan, M., et al. (2010). Insights into chemistry of biological materials: Newly discovered silica–aragonite–chitin biocomposites in demosponges. *Chemistry of Materials*, *22*, 1462–1471.

Ehrlich, H., Deutzmann, R., Brunner, E., Cappellini, E., Koon, H., Solazzo, C., et al. (2010). Mineralization of the metre-long biosilica structures of glass sponges is templated on hydroxylated collagen. *Nature Chemistry*, *2*, 1084–1088.

Ehrlich, H., Brunner, E., Simon, P., Bazhenov, V. V., Botting, J. P., Tabachnick, K. R., et al. Calcite reinforced silica–silica joints in the biocomposite skeleton of deep-sea glass sponges. *Advanced Functional Materials*, in press.

Gheysen, G., Ducheyne, P., Hench, L. L., & Meester, P. (1983). Bioglass composites: a potential material for dental application. *Biomaterials*, *4*, 81–84.

Heinemann, S., Heinemann, C., Ehrlich, H., Meyer, M., Baltzer, H., Worch, H., et al. (2007). A novel biomimetic hybrid material made of silicified collagen: perspectives for bone replacement. *Advanced Engineering Materials 2007*, *9*, 1061–1068.

Heinemann, S., Ehrlich, H., Knieb, C., & Hanke, T. (2007). Biomimetically inspired hybrid materials based on silicified collagen. *International Journal of Materials Research*, *98*, 603–608.

Hench, L. L., Splinter, R. J., Allen, W. C., & Greenlee, T. K. (1972). Bonding mechanisms at the interface of ceramic prosthetic materials. *Journal of Biomedical Materials Research*, *2*, 117–141.

Hench, L. L. (2009). Genetic design of bioactive glass. *Journal of European Ceramic Society*, *29*, 1257–1265.

Hong, Z., Reis, R. L., & Mano, J. F. (2008). Preparation and in vitro characterization of scaffolds of poly(L-lactic acid) containing bioactive glass ceramic nanoparticles. *Acta Biomaterialia*, *4*, 1297–1306.

Hulbert, S. F., Young, F. A., Mathews, R. S., Klawitter, J. J., Talbert, C. D., & Stelling, F. H. (1970). Potential of ceramic materials as permanently implantable skeletal prostheses. *Journal of Biomedical Materials Research*, *4*, 433–456.

Hunt, N. C., Smith, A. M., Gbureck, U., Shelton, R. M., & Grover, L. M. (2010). Encapsulation of fibroblasts causes accelerated alginate hydrogel degradation. *Acta Biomaterialia*, *6*, 3649–3656.

Ivanovski, S. (2009). Periodontal regeneration. *Australian Dental Journal*, *54*, 118–128.

Karageorgiou, V., & Kaplan, D. (2005). Porosity of 3D biomaterial scaffolds and osteogenesis. *Biomaterials*, *26*, 5474–5491.

Karring, T., Lindhe, J., & Cortellini, P. (1998). Regenerative periodontal therapy. In J. Lindhe (Ed.), *Clinical periodontology and implant dentistry* (pp. 597–638). Copenhagen: Munksgaard.

Kazy, S. K., Sar, P., Singh, S. P., Sen, A. K., & D'Souza, S. F. (2002). Extracellular polysaccharides of a copper-sensitive and a copper-resistant Pseudomonas aeruginosa strain: synthesis, chemical nature and copper binding. *World Journal of Microbiology & Biotechnology*, *18*, 583–588.

Kim, B. S., Park, I. K., Hoshiba, T., Jiang, H. L., Choi, Y. J., Akaikef, T., et al. (2011). Design of artificial extracellular matrices for tissue engineering. *Progress in Polymer Science*, *36*, 238–268.

Kokubo, T., & Takadama, H. (2006). How useful is SBF in predicting in vivo bone activity? *Biomaterials*, *27*, 2907–2915.

Kokubo, T., Kim, H. M., & Kawashita, M. (2003). Novel bioactive materials with different mechanical properties. *Biomaterials*, *24*, 2161–2175.

Liu, A., Hong, Z., Zhuang, X., Chen, X., Cui, Y., Liu, Y., et al. (2008). Surface modification of bioactive glass nanoparticles and the mechanical and biological properties of poly(L-lactide) composites. *Acta Biomaterialia*, *4*, 1005–1015.

Liuyun, J., Yubao, L., & Chengdong, L. (2009). A novel composite membrane of chitosan–carboxymethyl cellulose polyelectrolyte complex membrane filled with nano-hydroxyapatite I. Preparation and properties. *Journal of Materials Science: Materials in Medicine*, *20*, 1645–1652.

Lobel, K. D., & Hench, L. L. (1996). In vitro protein interactions with a bioactive gel–glass. *Journal of Sol–Gel Science and Technology*, *7*, 69–76.

Madhumathi, K., Binulal, N. S., Nagahama, H., Tamura, H., Shalumon, K. T., Selvamurugan, N., et al. (2009). Preparation and characterization of novel β-chitin-hydroxyapatite composite membranes for tissue engineering applications. *International Journal of Biological Macromolecules*, *44*, 1–5.

Madhumathi, K., Shalumon, K. T., Divya Rani, V. V., Tamura, H., Furuike, T., Selvamurugan, N., et al. (2009). Wet chemical synthesis of chitosan hydrogel–hydroxyapatite composite membranes for tissue engineering applications. *International Journal of Biological Macromolecules*, *45*, 12–15.

Melcher, A. H. (1976). On the repair potential of periodontal tissues. *Journal of Periodontology*, *47*, 256–260.

Misra, S. K., Ansari, T., Mohn, D., Valappil, S. P., Brunner, T. J., Stark, W. J., et al. (2010). Effect of nanoparticulate bioactive glass particles on bioactivity and cytocompatibility of poly(3-hydroxybutyrate) composites. *Journal of The Royal Society Interface*, *7*, 453–465.

Mohan, N., & Nair, P. D. (2005). Novel porous, polysaccharide scaffolds for tissue engineering applications. *Trends in Biomaterials and Artificial Organs*, *18*, 219–224.

Nandi, S. K., Kundu, B., Datta, S., De, D. K., & Basu, D. (2009). The repair of segmental bone defects with porous bioglass: an experimental study in goat. *Research in Veterinary Science*, *86*, 162–173.

Nyman, S., Lindhe, J., Karring, T., & Rylander, H. (1982). New attachment following surgical treatment of human periodontal disease. *Journal of Clinical Periodontology*, *9*, 290–296.

Peter, M., Sudheesh Kumar, P. T., Binulal, N. S., Nair, S. V., Tamura, H., & Jayakumar, R. (2009). Development of novel α-chitin/nanobioactive glass ceramic composite scaffolds for tissue engineering applications. *Carbohydrate Polymers*, *78*, 926–931.

Peter, M., Binulal, N. S., Nair, S. V., Selvamurugan, N., Tamura, H., & Jayakumar, R. (2010). Novel biodegradable chitosan–gelatin/nano-bioactive glass ceramic composite scaffolds for alveolar bone tissue engineering. *Chemical Engineering Journal*, *158*, 353–361.

Price, N., Bendall, S. P., Frondoza, C., Jinnah, R. H., & Hungerford, D. S. (1997). Human osteoblast-like cells (MG63) proliferate on a bioactive glass surface. *Journal of Biomedical Materials Research*, *37*, 394–400.

Reynolds, M. A., Aichelmann-Reidy, M. E., & Branch-Mays, G. L. (2010). Regeneration of periodontal tissue: bone replacement grafts. *Dental clinics of North America*, *54*, 55–71.

Rezwan, K., Chen, Q., Blaker, J. J., & Boccaccini, A. R. (2006). Biodegradable and bioactive porous polymer/inorganic composite scaffolds for bone tissue engineering. *Biomaterials*, *27*, 3413–3431.

Roman, J., Padilla, S., & Vallet-Regý, M. (2003). Sol–gel glasses as precursors of bioactive glass ceramics. *Chemistry of Materials*, *15*, 798–806.

Sowmya, S., Sudheesh Kumar, P. T., Chennazhi, K. P., Nair, S. V., Tamura, H., & Jayakumar, R. (2011). Biocompatible β-chitin hydrogel/nanobioactive glass ceramic nanocomposite scaffolds for periodontal bone regeneration. *Trends in Biomaterials and Artificial Organs*, *25*, 1–11.

Sudheesh Kumar, P. T., Sowmya, S., Vinoth-Kumar, L., Tamura, H., Nair, S. V., & Jayakumar, R. (2011). β-Chitin hydrogel/nano hydroxyapatite composite scaffolds for tissue engineering applications. *Carbohydrate Polymers*, *85*, 584–591.

Tan, H., & Kacey, G. M. (2010). Injectable biodegradable hydrogels for tissue engineering applications. *Materials*, *3*, 1746–1767.

Valerio, P., Pereira, M. M., Goes, A. M., & Leite, M. F. (2004). The effect of ionic products from bioactive glass dissolution on osteoblast proliferation and collagen production. *Biomaterials*, *25*, 2941–2948.

Walker, J. M. (1994). The bicinchoninic acid (BCA) assay for protein quantitation. In J. M. Walker (Ed.), *Basic protein and peptide protocols* (pp. 5–8). Totowa NJ: Humana Press Inc.

Wang, L., Shelton, R. M., Cooper, P. R., Lawson, M., Triffitt, J. T., & Barralet, J. E. (2003). Evaluation of sodium alginate for bone marrow cell tissue engineering. *Biomaterials*, *24*, 3475–3481.

Wang, Z. Y., Zhang, Q. Z., Konno, M., & Saito, S. (1993). Sol–gel transition of alginate solution by the addition of various divalent cations: ^{13}C-NMR spectroscopic study. *Biopolymers*, *33*, 703–711.

Xia, W., & Chang, J. (2007). Preparation and characterization of nano-bioactive-glasses (NBG) by a quick alkali-mediated sol–gel method. *Materials Letters*, *61*, 3251–3253.

Xynos, I. D., Edgar, A. J., Buttery, L. D. K., Hench, L. L., & Polak, J. M. (2000). Ionic products of bioactive glass dissolution increase proliferation of human osteoblasts and induce insulin-like growth factor II mRNA expression and protein synthesis. *Biochemical and Biophysical Research Communications*, *276*, 461–465.